2022 IEEE 5th International Conference on Soft Robotics (RoboSoft)
April 4-8, 2022, Edinburgh, UK

Self-Sensing, Stretchable, Active Circuit Arrays: Liquid Metal Paste as a Combination Interconnect and Strain Sensor

Callen Votzke[1], Yiğit Mengüç[2], and Matthew L. Johnston[1]

***Abstract*— Stretchable electrical interconnects and substrate materials are increasingly used to create flexible and conformable electronic systems for soft robotics, smart textiles, and wearable devices. Wires fabricated using composite or liquid conductive inks encapsulated in silicone enable high strain and are mechanically robust. The resistance of these interconnects increases with strain, which can present challenges for power delivery and signaling among electronic components. However, this effect can be used directly to estimate strain within a stretchable circuit without the need for additional sensor components. In this work, we present an approach for fabricating fully-stretchable, multi-layer active circuit arrays in silicone using liquid metal paste interconnects, in which power and data wires are re-purposed as strain sensors to estimate substrate deformation. As a proof-of-principle, we demonstrate a 3×3 active circuit array that self-senses relative voltage supply at each node to estimate deformation and consumes less than 10 mA per node. Each node is digitally addressable and performs both analog measurement and digital conversion. All interconnects are fabricated using liquid metal paste, and power, data, and sensing are performed over a shared, four-wire interface in this multi-layer stretchable printed circuit board.**

I. Introduction

Stretchable electronics are a promising paradigm for enabling new wearable devices and soft robots by giving electronics the ability to be worn like a second skin, conforming to and moving with the wearer, and with sensors distributed throughout. To do so, the conventional patterned copper on fiberglass printed circuit board (PCB) is replaced with a stretchable interconnect material encapsulated in a stretchable substrate, commonly silicone. Materials used for stretchable interconnects largely depend on the desired maximum strain limits, ranging from patterned solid metal serpentine traces and coils [1] to gallium-based metals that are liquid at room temperature [2]. Alloys of gallium, indium, and tin are an increasingly common choice for an interconnect material with high strain capability (>1000% [3]); such liquid metals have been used in many demonstrated approaches for interconnect patterning, including direct writing [4], stenciling [5], soft lithography [6], and selective wetting [7].

Fully-integrated stretchable circuits with touch-sensing capability have previously been applied to soft robots [8], [9] and as soft skins [10]. While stretchable sensors for measuring strain, pressure, or touch have existed for some time, they rely on dedicated sensing elements [11]–[14] or external sensors for position detection [15], [16].

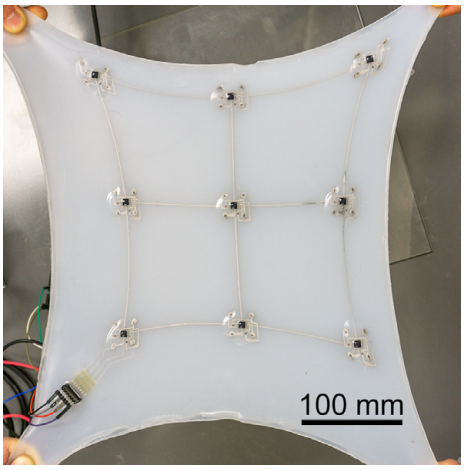

Fig. 1: A fully-stretchable, self-sensing 3×3 active circuit array farbicated as a multi-layer stretchable printed circuit board (PCB). As the grid is deformed, coordination between analog measurement circuitry and embedded microcontrollers at each node can detect small changes in interconnect resistance of the liquid metal wires to estimate deformation. By re-purposing the wires used for digital communication among nodes for this measurement, the need for separate strain-sensing elements is eliminated.

In this work, we demonstrate the design and implementation of a self-sensing stretchable wire grid that uses interconnect strain to estimate internal deformation. Embedded active digital and analog electronics at each grid node within the "stretchable PCB" provide strain estimation, and all interconnects for the stretchable printed circuits are formed using patterned liquid metal paste. This fully-integrated approach is demonstrated using a 3×3 node array, as illustrated in Fig. 1, and demonstrates the ability to estimate interconnect strain by re-purposing power and data wires, rather than requiring a separate, discrete sensing element. This scalable approach may provide a foundation for future development of proprioceptive soft skins that can provide additional sensors at each node (accelerometers, temperature, etc.) in addition to self-sensing relative displacement between nodes.

II. Overview of Self-Sensing Stretchable Grid

A. Theory of Operation

A stretchable, self-sensing network is formed by an array of individually-addressable electronic nodes connected by liquid metal paste wires encapsulated in silicone. This method supports high strains of at least 150 % [17].

This work is supported in part by the Semiconductor Research Corporation (SRC) through the SRC Graduate Fellowship Program, and in part by the DOE/NNSA Office of Defense Nuclear Nonproliferation Research and Development.

[1]Callen Votzke and Matthew L. Johnston are with the School of Electrical Engineering and Computer Science and the Collaborative Robotics and Intelligent Systems Institute, Oregon State University, Corvallis, OR 97331, USA. votzkec@oregonstate.edu

[2]Yiğit Mengüç is with Facebook Reality Labs, Redmond, WA, 98052.

2022 IEEE 5th International Conference on Soft Robotics (RoboSoft) | 978-1-6654-0828-8/22/$31.00 ©2022 IEEE | DOI: 10.1109/ROBOSOFT54090.2022.9762152

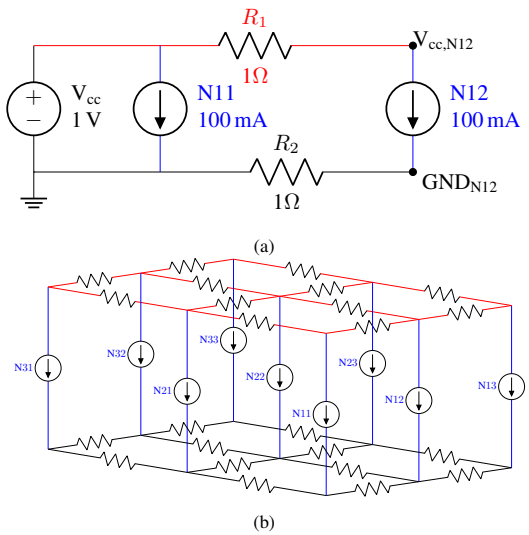

Fig. 2: Electrical diagram for theory of operation. a) Simplified case with two nodes, N_{11} and N_{12}. b) Full model of a 3×3 stretchable grid. The top grid, shown in red, is a model of V_{cc}; the bottom grid, shown in black, is a model of GND. Each node, labeled with its address, is modeled as a current load between the two grids. A voltage source, not shown, is applied at node 11.

The gallium-based liquid metal paste has a bulk conductivity (ρ^{-1}) of approximately 10 % that of copper [18], giving the wires a small but non-negligible resistance. This resistance is low enough to not inhibit circuit functionality or interfere with digital communication, and it minimizes resistive power losses in the interconnects. It is large enough, however, to cause small but measurable voltage drops across the array that vary with strain, which can be used to self-sense physical deformation using the circuit power and data wires directly; no additional strain sensors are required. This is made possible by incorporating active electronics at each grid node, including both analog measurement and digital communication capabilities.

A quadratic change in resistance with strain stems from wire geometry, as the bulk conductivity of the paste, $1/\rho$, does not change with deformation and has negligible position-dependent hysteresis [19]. As the wire length, l, increases with stretch, the cross-sectional area of the wire, A, is also reduced. As $R = \rho \frac{l}{A}$, the resistance of the wire is therefore proportional to the square of the relative stretch; a wire stretched to twice its original length will have four times its original resistance.

Power is supplied to the arrayed circuit by two fully-connected wire grids: one providing voltage supply (V_{cc}), and one providing a common ground reference and current return (GND). When used to supply power, liquid metal traces carry non-negligible current and therefore must be considered as a grid of individual variable resistors to account for the voltage drops across the grid. As the V_{cc} and GND wires are physically superimposed in different electrical layers of the stretchable grid, paired power and ground wires are assumed to have the same relative deformation at all times. Powered circuitry at each node, in turn, can be modeled as a current load at a node-local supply voltage. As

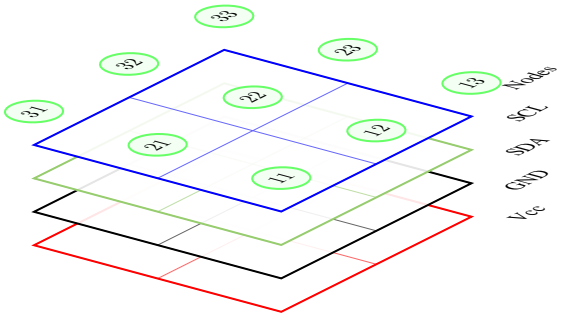

Fig. 3: Five-layer construction used for the stretchable grid. The top layer is used exclusively for the embedded components, while the other four layers are a grid of liquid metal paste used for each of the four wires required by each node: two wires for power (V_{cc} and GND), and two wires for I^2C communication (Serial Data / SDA, and Serial Clock / SCL). The address of each node, from 11 to 33, is shown on the top layer.

each node draws current, this causes a voltage drop between each node and the supply; as relative interconnect strain increases, so does this voltage drop.

A simplified case with only two nodes illustrates this operation in Fig. 2a. Power supply rails V_{cc} (1 V) and GND (0 V) are applied at node N_{11}. The current supplying N_{12} must pass through two stretchable wires, which each have an unstretched resistance of 1 Ω. If each node has a current draw of 100 mA,

$$V_{R1,R2} = R_1 \times I_{N12} = 1\Omega \times 100\,\text{mA} = 100\,\text{mV}$$
$$V_{cc,N12} = V_{cc,N11} - V_{R1} = 1\,\text{V} - 100\,\text{mV} = 900\,\text{mV}$$
$$GND_{N12} = GND_{N11} + V_{R2} = 0\,\text{V} + 100\,\text{mV} = 100\,\text{mV}$$
$$V_{N12} = V_{cc,N12} - GND_{N12} = 800\,\text{mV}$$

and N_{12} sees an effective supply voltage of 800 mV due to the voltage drop in both V_{cc} and GND. If R1 and R2 are both increased to 2 Ω, indicating a strain of ∼41%, $V_{R1,R2}$ = 200 mV, and the effective supply voltage at N_{12} has decreased to 600 mV. For this example, current values have been increased to clearly highlight the effect; as implemented, circuits at each node draw a few milliamps, and changes in node-local supply voltage are on the order of a few millivolts under normal operation.

While the complexity of solving for deformation-induced voltage drop increases for larger arrays due to the presence of multiple parallel conductive paths to each node, the concept of the relative voltage drop at each node remains the same. A simplified model of a larger 3×3 grid is shown in Fig. 2b; this model was translated into SPICE and used to compare to the experimental results in Section IV-A. By measuring the voltage drop at each node relative to the supply, the deformation of the grid can be estimated.

B. Self-Sensing Grid Implementation and Operation

For this implementation, each node consists of a microcontroller (Microchip ATtiny85) and a switchable resistive load. Each node connects to the other nodes through electrical vias to four independent, fully-connected wire grids, illustrated in Figs. 3 and 6: two wires for power (V_{cc} and GND), and two wires for digital I^2C communication (Serial Data / SDA, and

Serial Clock / SCL) on a grid-wide bus. Note that there are no dedicated strain sensors: the supply and data conductor grids are used to estimate the deformation of the sheet.

Each node connects to the four underlying grid layers through electrical vias, as shown in Fig. 4a. All electrical interconnects are made of liquid metal paste encapsulated in silicone, as detailed in Section III. A separate, off-grid microcontroller board is used to translate the I^2C bus data and commands into serial for capture and control by a laptop. While the current implementation includes only circuits for estimation of wire strain, additional sensors and actuators could be easily added to each node in future iterations.

The relaxed (unstretched) resistance of each of the liquid metal wires between each node is approximately 0.5 Ω. The microcontroller at each node has a current draw of approximately 1.1 mA at 5 V, with the ability to toggle the connection of a local 1 kΩ resistor between V_{cc} and ground. This toggle is done by I^2C command to each node. With the load resistor on, the active circuitry is effectively a 6.1 mA current load at each node with a 5 V supply. The load resistor boosts the voltage drop at each node to increase sensitivity by 6X (6.1 mA versus 1.1 mA), which is only needed during measurement of deformation; the load can be toggled off between measurements to save power.

To further increase the sensitivity to small changes in grid shape, the voltage drop between two nodes is measured directly. A built-in 10-bit analog-to-digital converter (ADC) in each microcontroller is used in differential mode, where it measures the difference between two inputs, rather than the difference between a single input and the node's local ground. With a 1.1 V internal ADC reference and the application of an internal 20X gain stage, this provides an effective resolution of ∼0.05 mV. Compared to indirectly measuring voltage drops by subtracting measurements of supply voltage taken by each node, which has a resolution of only 5 mV, measuring directly provides a 100X sensitivity improvement.

To make this differential measurement, the two ADC inputs must be connected to the node-local V_{cc} and to the V_{cc} of the target node, respectively. In lieu of direct connections to the V_{cc} of each node, which would require significantly more wires, the circuit is able to re-use the two digital I^2C communication grids, SDA and SCL, to perform the differential reading. This transaction is shown in Fig. 4e for the direct differential measurement of $V_{cc,N11}$ and $V_{cc,N33}$ using the microcontroller ADC located at node 11.

The external controller first sends a command to node 11 to take a differential measurement with node 33. Node 11 assumes ownership of the I^2C bus from the controller and transmits a command to node 33 to enter signalling mode. Both node 11 and 33 then disable their respective I^2C transceivers, freeing the SDA and SCL grids to be used. Node 11 asserts a logical 1 on the SCL grid, to which node 33, now in signalling mode, responds by asserting a logical 1 on the SDA grid. Each logical 1, however, is at the node-local V_{cc}, and the voltage level of SDA is now $V_{cc,N33}$.

At this point, the two differential ADC pins (Fig. 4d) of node 11 are connected to $V_{cc,N11}$ (ADC+) and the SDA grid

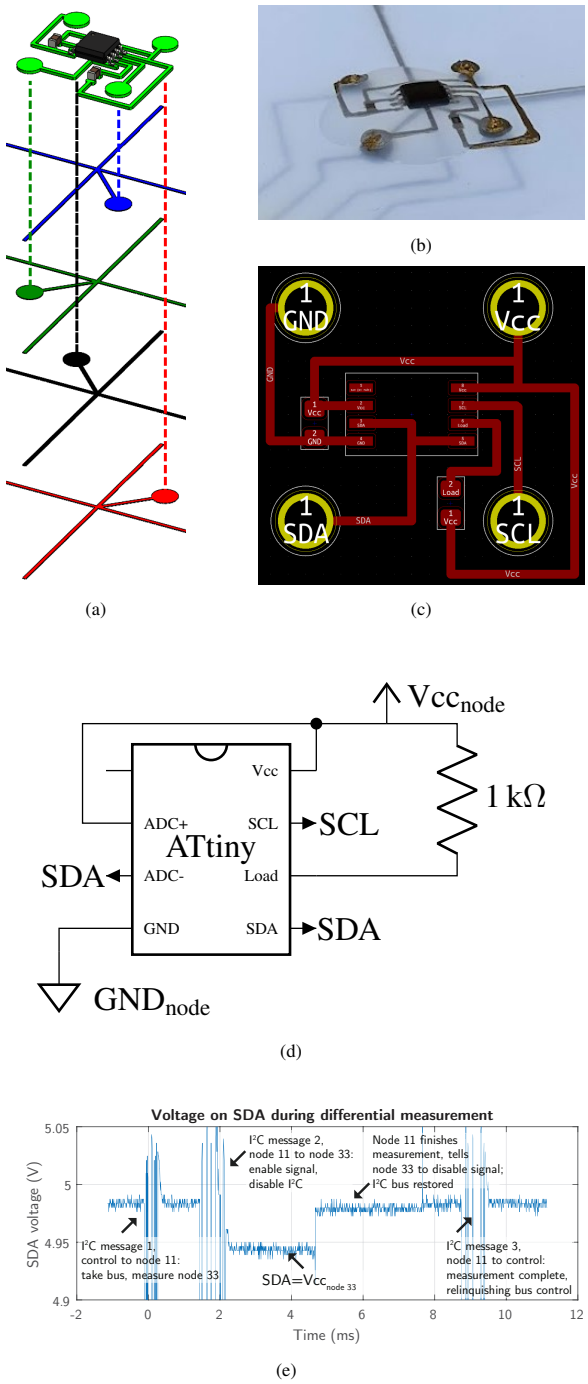

Fig. 4: Overview of an individual node. a) Cutaway view of a single node within the stretchable grid. The top layer, which contains all the active circuitry and embedded components, connects to each of the four grid layers (from bottom to top: V_{cc}, ground, SDA, and SCL with vias (illustrated as dashed lines) in the silicone. As this cutaway shows the center node of the grid (node 22), the grid lines extend to nodes in all four cardinal directions. b) A close-up photo of a node showing the strain isolation silicone. c) The circuit layout for a single node. d) The electrical schematic for a single node. e) An oscilloscope capture of the SDA line during differential measurement. Between 2 ms and 4.5 ms, the SDA line is pulled to the V_{cc} of the node under measurement.

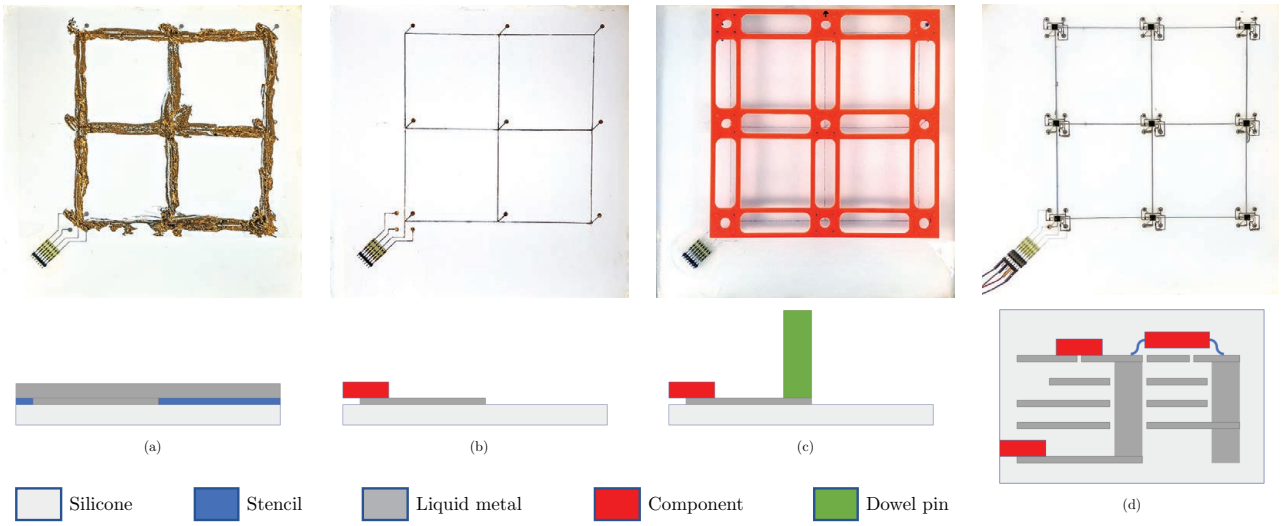

Fig. 5: Stenciling process for fabrication of multi-layer liquid metal circuit with multiple vias.

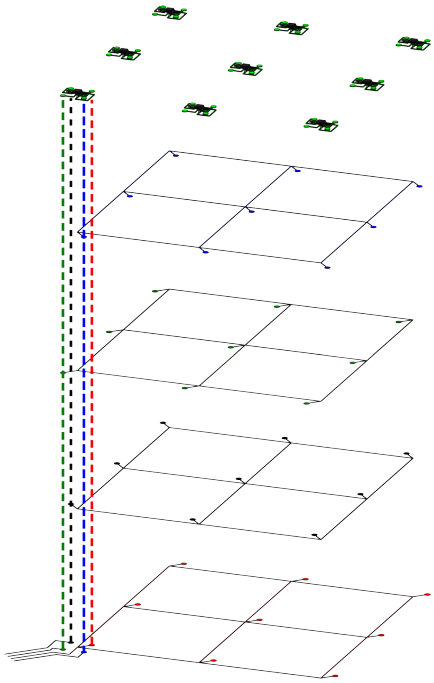

Fig. 6: Exploded CAD diagram showing the five layers of the stretchable grid design: four fully-connected grids for power and digital communications, and a top layer for local connections to embedded components for each node. Vias for node 11 are shown as dotted lines to denote top layer connections to each of the grids.

(ADC-), which is now held at $V_{cc,N33}$. Node 11 then measures the differential voltage between ADC+ and ADC-. Once the reading is completed, node 11 de-asserts SCL, causing node 33 to de-assert SDA; both re-enable their I^2C transceivers, and node 11 informs the external controller that it can retake command of the bus. The controller then queries node 11 for the $V_{cc,N11}$-$V_{cc,N33}$ differential measurement.

This process can be repeated to measure the difference in node-local supply voltage between any two nodes. This scheme is made possible by re-purposing the digital bus

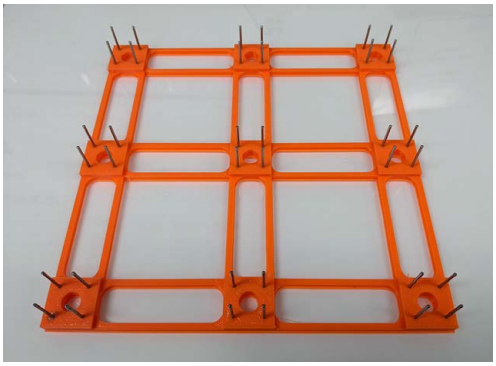

Fig. 7: The 3D-printed jig used to form all 36 via holes required for the stretchable grid: 9 nodes with 4 vias each. Each hole is formed by a 1 in.-long, 1/16 in. diameter dowel pin that has been press-fit into the jig. The jig is skeletonized so that uncured silicone can be poured through the jig without disturbing its position.

lines, as ADC measurements draw negligible current and induce negligible additional voltage drop compared to the current-carrying voltage supply wires.

C. Stretchable Grid Simulator

For a stretchable circuit, the components and traces are fully encapsulated within silicone, making in-situ reprogramming of each microcontroller infeasible. In order to test our grid design and the associated embedded firmware prior to encapsulation, a rigid "stretchable simulator" board was made using conventional PCB technology. It features a 4×4 grid layout with swappable node daughterboards and adjustable resistances on all four wires between nodes. This allows for standalone firmware debugging and testing using known grid resistances prior to stretchable circuit fabrication.

III. Self-Sensing Grid - Manufacture

The stretchable grid is made of five layers: four fully-connected grids (V_{cc}, GND, SDA, and SCL) used as interconnects between nodes, and a top layer containing embedded electronic components, component-level interconnect

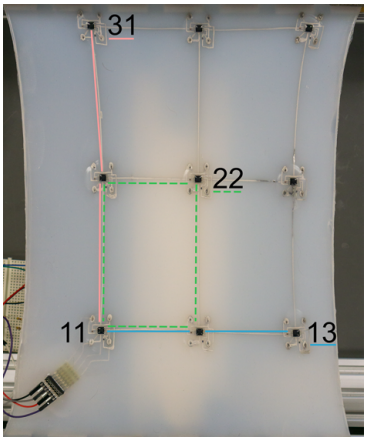

(a)

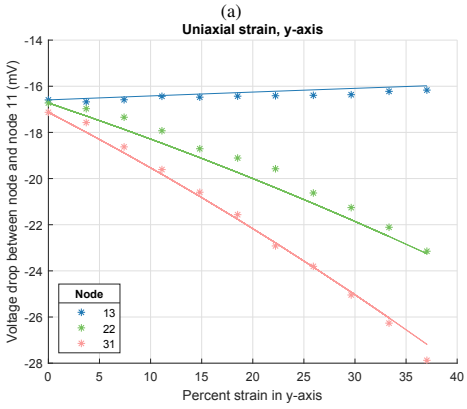

(b)

Fig. 8: Uniaxial strain in the y-axis. a) Illustrated shortest paths between node 11 and nodes 13, 22, and 31. b) Data from uniaxial stretch testing, with overall percent strain in the y direction versus the voltage drop between node 11 and nodes 13, 22, and 31.

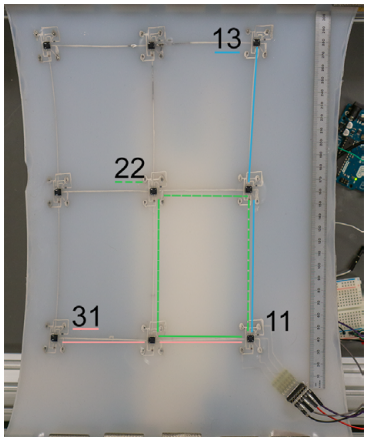

(a)

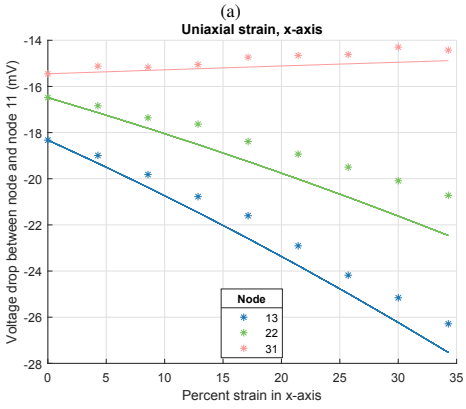

(b)

Fig. 9: Uniaxial strain in the x-axis. a) Illustrated shortest paths between node 11 and nodes 13, 22, and 31. b) Data from uniaxial stretch testing, with overall percent strain in the x direction versus the voltage drop between node 11 and nodes 13, 22, and 31.

routing, and local strain isolation for each node. Fig. 6 provides an exploded diagram of the CAD model used for the liquid metal wires. The manufacturing process is shown in Fig. 5 and extends upon our earlier work [17].

First, a layer of soft Ecoflex 00-30 silicone is cast, forming a base upon which liquid metal paste can be stenciled. A stencil for the first layer is cut from an acetate sheet using a knife plotter (Silhouette Cameo 3) and is aligned to the silicone base. The liquid metal paste is then applied (Fig. 5a), and a squeegee is used to remove the excess. The stencil is removed, revealing the traces for the first layer. A swab lightly wetted with solvent (Simple Green) can be used to reclaim unused paste left on the stencil for reuse. Any components, such as the passive four-wire connector PCB on the bottom layer, can be inserted at this stage (Fig. 5b).

Vertical electrical connections, or vias, between layers are formed by creating small voids in successive silicone layers. A 3D-printed jig holding dowel pins in the position of each via (Fig. 7) is placed onto the first layer of liquid metal (Fig. 5c), and liquid silicone is poured around it. Once the silicone for the second layer base is cured, the jig is removed; as this design uses through-vias (vertical connections penetrate through, but not necessarily connect to, all layers), the voids created in the second layer can be used to repeatably realign the pin jig for all successive layers.

The process can be repeated for multi-layer circuit fabrication by applying another stencil, more liquid metal paste, any components, and the pin jig again. For the 5-layer stretchable PCB shown here, after the fifth and final liquid metal layer is stenciled, the vias are filled with liquid metal and tested for continuity. Circuit components are individually encapsulated by a small amount of Dragon Skin 10, which is slightly stiffer than the Ecoflex 00-30, to provide local strain isolation. A final layer of Ecoflex silicone then fully encapsulates all the components and liquid metal (Fig. 5d).

IV. Self-Sensing Grid - Experimental Testing

A. Uniaxial Stretch

Functionality of the stretchable grid was first validated using uniaxial strain in each of the x- and y-axes. Two opposite edges of the grid were clamped into a custom, uniaxial stretching machine (described in [20]), as shown in Fig. 10a, and the top edge was moved to a known displacement by a calibrated lead screw. Due to the hyperelastic nature of the silicone, displacement of the ends does not perfectly correspond with the internal strain in the circuit; engineering strain is instead measured photographically by comparing the stretched and unstretched lengths.

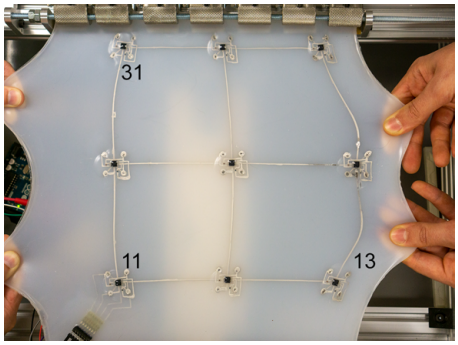

(a)

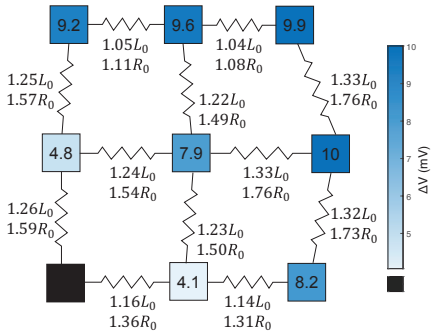

(b)

Fig. 10: Stretchable grid under biaxial strain: a) Photo of x- and y-axis strain applied to the stretchable grid. b) Internally-measured change in relative supply voltage to node 11 due to strain. Each wire is labeled with relative change in length and associated change in resistance from nominal.

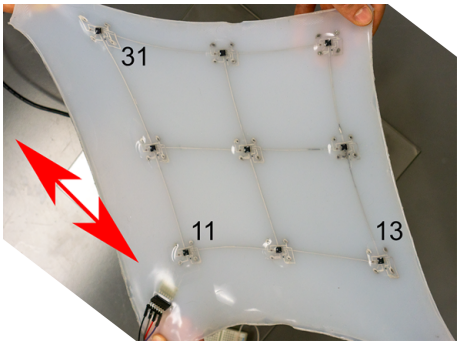

(a)

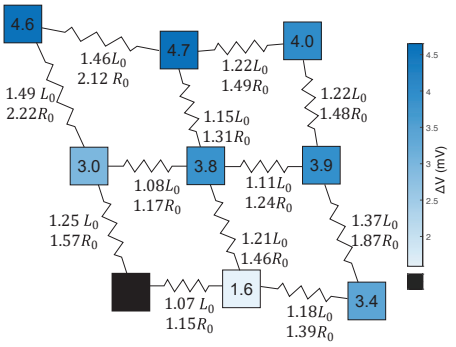

(b)

Fig. 11: Stretchable grid under corner-to-corner strain: a) Photo of off-axis strain applied to the stretchable grid (arrows denote strain direction). b) Internally-measured change in relative supply voltage to node 11 due to strain. Each wire is labeled with relative change in length and associated change in resistance from nominal.

To understand the response of the stretchable grid to deformation, it is helpful to look at the three nodes that have the same total interconnect length ("Manhattan distance") from the origin node 11: nodes 13, 22, and 31. This is illustrated in Figs. 8 and 9 for the y-axis and x-axis uniaxial stretch cases, respectively. The Manhattan distance corresponds to the minimum number of stretchable links between the node and the origin node; as these links deform, the voltage drop between nodes will change. Each node has a different configuration of its shortest path: node 13 has two links in the x-axis, node 22 has two parallel paths of one link each in x and y, and node 31 has two links in the y-axis; as such, the response of each node varies with strain direction. While the response is not purely dictated by the shortest path, as there are multiple parallel paths to each node, it is a useful simplification for understanding the response of the grid.

The response of nodes 13, 22, and 31 for uniaxial stretch in y is shown in Fig. 8b. The overall y-axis strain on the device, measured between nodes 11 and 31, is plotted against the voltage drop between node 11 and the measured 'target' node. Averaged data from five stretch-relax cycles are plotted as points; the simulated grid response using the the SPICE model (Fig. 2b) is plotted as lines. All three nodes have approximately the same voltage drop at zero strain, as expected, as they have approximately the same shortest-path resistance ($\sim$0.5 Ω per segment). The simulated response lines have been calibrated to this zero strain measurement.

The voltage drop to both node 22 and node 31 increases with stretch, with the drop to node 31 increasing at a larger rate because both wires in the shortest path are parallel to the stretch direction. Node 22, by contrast, has only one wire parallel to the stretch direction, and thus changes at a reduced proportion. Nodes 11 and 13, as is seen in Fig. 8a, actually move slightly closer together; the distance between these at 35 % y-axis device strain is only 90% of nominal. Hence, their local strain is actually negative, and the resistance of the wires between nodes 11 and 13 decreases. This is correctly reflected in the fit line from SPICE.

When the grid is rotated 90 degrees in the stretcher, such that the grid is now strained uniaxially in the x-axis, the responses of the nodes switch; this is shown in Fig. 9b. The same decrease in voltage drop for nodes perpendicular to the strain direction is seen because nodes 11 and 31 move closer together (Fig. 9a). This, again, is a decrease to approximately 90% of the nominal distance between nodes 11 and 31. Similarly, the voltage drop to node 22 increases at a lower proportion than the drop to node 13.

By comparing the responses at the two opposite corners, it is possible to estimate the uniaxial strain experienced by the grid: the drop to node 31 will increase with strain in y, while the drop to node 13 will increase with strain in x.

B. Other Stretch Conditions

While convenient for controlled measurements, strain rarely comes in purely controlled, uniaxial forms. Thus, the

stretchable grid has been tested in two other conditions to demonstrate its ability to sense other planar deformations: biaxial, where the grid is strained simultaneously in x and y, and corner-to-corner, where the grid is strained in a single axis 45 degrees from x and y.

Fig. 10a shows the stretchable grid strained in the y-axis by the uniaxial stretcher and in the x-axis by hand. The heatmap in Fig. 10b shows the relative change in node voltage drop between the relaxed grid and the biaxially-strained grid with node 11 as the reference node. As expected, nodes farther from node 11 experience a larger voltage drop, with node 23 (directly above node 13) having the largest deformation and exhibiting the largest voltage difference.

Fig. 11a shows the stretchable grid strained diagonally corner-to-corner, as noted by the arrows. The other two corners are supported but not strained. The heatmap in Fig. 11b shows the change in node voltage drop between the relaxed grid and the grid stretched at opposite corners, estimating relative strain from node 11 to target nodes.

V. Conclusion

We have presented an approach for fabricating fully-stretchable, multi-layer active circuit arrays in silicone using liquid metal paste interconnects, in which power and data wires are re-used as strain sensors to estimate substrate deformation. A 3×3 active circuit array was fabricated and characterized as a proof-of-principle. The array self-senses relative voltage supply at each node to estimate deformation and consumes less than 10 mA per node. Each node is digitally addressable from a shared bus and performs both analog measurement and digital conversion. All interconnects are fabricated using liquid metal paste, and all power, data, and sensing are performed over a shared four-wire interface. Both uniaxial and biaxial characterizations are shown, illustrating the potential of the presented approach for self-measuring deformation within a stretchable circuit. We also note that all fabrication can be completed using low-cost, consumer-grade 'maker' tools.

The fully-stretchable, shared bus approach is highly scalable and can also support the inclusion of additional sensors or actuators into the stretchable printed circuits. A potential future application would be as a distributed proprioception network within a soft actuator, where each node can measure its own orientation in space as well as the relative displacement from other nodes. Despite using only four wires, the design can be expanded to more than 100 nodes using a single I^2C bus. As implemented, this approach requires only low-cost, low-power microcontrollers and passive components to perform all measurements. Further development will focus on the continued characterization of grid responses to varied strain conditions, while continuing to improve grid density and measurement capabilities.

References

[1] Z. Fan, Y. Zhang, Q. Ma, F. Zhang, H. Fu, K.-C. Hwang, and Y. Huang, "A finite deformation model of planar serpentine interconnects for stretchable electronics," *International Journal of Solids and Structures*, vol. 91, pp. 46–54, Aug. 2016.

[2] S.-Y. Tang, C. Tabor, K. Kalantar-Zadeh, and M. D. Dickey, "Gallium Liquid Metal: The Devil's Elixir," *Annual Review of Materials Research*, vol. 51, no. 1, pp. 381–408, July 2021.

[3] S. Zhu, J. H. So, R. Mays, S. C. Desai, W. R. Barnes, B. Pourdeyhimi, and M. D. Dickey, "Ultrastretchable fibers with metallic conductivity using a liquid metal alloy core," *Advanced Functional Materials*, vol. 23, no. 18, pp. 2308–2314, 2013.

[4] A. D. Valentine, T. A. Busbee, J. W. Boley, J. R. Raney, A. Chortos, A. Kotikian, J. D. Berrigan, M. F. Durstock, and J. A. Lewis, "Hybrid 3D Printing of Soft Electronics," *Advanced Materials*, vol. 29, no. 40, pp. 1–8, 2017.

[5] Q. Zhang, Y. Gao, and J. Liu, "Atomized spraying of liquid metal droplets on desired substrate surfaces as a generalized way for ubiquitous printed electronics," *Applied Physics A: Materials Science and Processing*, vol. 116, no. 3, pp. 1091–1097, 2014.

[6] Y.-L. Park, B.-R. Chen, and R. J. Wood, "Design and Fabrication of Soft Artificial Skin Using Embedded Microchannels and Liquid Conductors," *IEEE Sensors Journal*, vol. 12, no. 8, pp. 2711–2718, Aug. 2012.

[7] K. B. Ozutemiz, J. Wissman, O. B. Ozdoganlar, and C. Majidi, "EGaIn-Metal Interfacing for Liquid Metal Circuitry and Microelectronics Integration," *Advanced Materials Interfaces*, vol. 5, no. 10, p. 1701596, May 2018.

[8] T. Hellebrekers, K. B. Ozutemiz, J. Yin, and C. Majidi, "Liquid Metal-Microelectronics Integration for a Sensorized Soft Robot Skin," in *2018 IEEE/RSJ International Conference on Intelligent Robots and Systems (IROS)*. Madrid: IEEE, Oct. 2018, pp. 5924–5929.

[9] J. Yin, T. Hellebrekers, and C. Majidi, "Closing the Loop with Liquid-Metal Sensing Skin for Autonomous Soft Robot Gripping," in *2020 3rd IEEE International Conference on Soft Robotics (RoboSoft)*. New Haven, CT, USA: IEEE, May 2020, pp. 661–667.

[10] B. Shih, D. Shah, J. Li, T. G. Thuruthel, Y.-L. Park, F. Iida, Z. Bao, R. Kramer-Bottiglio, and M. T. Tolley, "Electronic skins and machine learning for intelligent soft robots," *Science Robotics*, vol. 5, no. 41, p. eaaz9239, Apr. 2020.

[11] S. Din, W. Xu, L. K. Cheng, and S. Dirven, "A Stretchable Multimodal Sensor for Soft Robotic Applications," *IEEE Sensors Journal*, vol. 17, no. 17, pp. 5678–5686, Sept. 2017.

[12] O. A. Araromi, M. A. Graule, K. L. Dorsey, S. Castellanos, J. R. Foster, W.-H. Hsu, A. E. Passy, J. J. Vlassak, J. C. Weaver, C. J. Walsh, and R. J. Wood, "Ultra-sensitive and resilient compliant strain gauges for soft machines," *Nature*, vol. 587, no. 7833, pp. 219–224, Nov. 2020.

[13] T. G. Thuruthel, B. Shih, C. Laschi, and M. T. Tolley, "Soft robot perception using embedded soft sensors and recurrent neural networks," *Science Robotics*, vol. 4, no. 26, p. eaav1488, Jan. 2019.

[14] T. Kim, S. Lee, T. Hong, G. Shin, T. Kim, and Y.-L. Park, "Heterogeneous sensing in a multifunctional soft sensor for human-robot interfaces," *Science Robotics*, vol. 5, no. 49, p. eabc6878, Dec. 2020.

[15] Y. Jin, Y. Lin, A. Kiani, I. D. Joshipura, M. Ge, and M. D. Dickey, "Materials tactile logic via innervated soft thermochromic elastomers," *Nature Communications*, vol. 10, no. 1, p. 4187, Dec. 2019.

[16] M. Hofer, C. Sferrazza, and R. D'Andrea, "A Vision-based Sensing Approach for a Spherical Soft Robotic Arm," *arXiv:2012.06413 [cs]*, Dec. 2020.

[17] C. Votzke, N. Alteir, Y. Menguc, and M. L. Johnston, "Stenciled Liquid Metal Paste for Robust Stretchable Electrical Interconnects," in *2021 IEEE International Conference on Flexible and Printable Sensors and Systems (FLEPS)*. Manchester, United Kingdom: IEEE, June 2021, pp. 1–4.

[18] U. Daalkhaijav, O. D. Yirmibesoglu, S. Walker, and Y. Mengüç, "Rheological Modification of Liquid Metal for Additive Manufacturing of Stretchable Electronics," *Advanced Materials Technologies*, vol. 1700351, pp. 1–9, 2018.

[19] C. Votzke, U. Daalkhaijav, Y. Menguc, and M. L. Johnston, "3D-Printed Liquid Metal Interconnects for Stretchable Electronics," *IEEE Sensors Journal*, vol. 19, no. 10, pp. 3832–3840, May 2019.

[20] C. Votzke, K. Clocker, Y. Menguc, and M. L. Johnston, "Electrical Characterization of Stretchable Printed Liquid Metal Interconnects under Repeated Cyclic Loading," in *2019 IEEE International Conference on Flexible and Printable Sensors and Systems (FLEPS)*. Glasgow, United Kingdom: IEEE, July 2019, pp. 1–3.